MOLECULAR BIOLOGY

Chromatin expansion microscopy reveals nanoscale organization of transcription and chromatin

Mark E. Pownall[1]*, Liyun Miao[1]*, Charles E. Vejnar[1], Ons M'Saad[2,3], Alice Sherrard[1], Megan A. Frederick[4], Maria D. J. Benitez[1], Curtis W. Boswell[1], Kenneth S. Zaret[4], Joerg Bewersdorf[2,3,5,6,7], Antonio J. Giraldez[1,8,9]*

Nanoscale chromatin organization regulates gene expression. Although chromatin is notably reprogrammed during zygotic genome activation (ZGA), the organization of chromatin regulatory factors during this universal process remains unclear. In this work, we developed chromatin expansion microscopy (ChromExM) to visualize chromatin, transcription, and transcription factors in vivo. ChromExM of embryos during ZGA revealed how the pioneer factor Nanog interacts with nucleosomes and RNA polymerase II (Pol II), providing direct visualization of transcriptional elongation as string-like nanostructures. Blocking elongation led to more Pol II particles clustered around Nanog, with Pol II stalled at promoters and Nanog-bound enhancers. This led to a new model termed "kiss and kick", in which enhancer–promoter contacts are transient and released by transcriptional elongation. Our results demonstrate that ChromExM is broadly applicable to study nanoscale nuclear organization.

Upon fertilization, embryos undergo transcriptional and cellular reprogramming to form a totipotent zygote (1–5). This reprogramming results in the transcriptional activation of genes required to initiate zygotic development. During this process, pioneer factors open the chromatin, recruit RNA polymerase II (Pol II), and activate transcription (6–9). However, the molecular organization of these factors during genome activation remains unclear. Nanoscale visualization of transcription and chromatin with current super-resolution approaches is limited by their ability to analyze nanoscale structure at the whole-nucleus scale, particularly in vivo. Alternatively, chromatin electron microscopy and tomography (ChromEMT) (10) provides nanometer resolution but lacks the multilabel imaging required to identify specific regulatory interactions. To overcome these limitations, we combined pan–expansion microscopy (pan-ExM) (11) with multimodal protein, RNA, and DNA labeling to resolve the nanoscale organization of chromatin, transcriptional activators, and transcription in a method that we term chromatin expansion microscopy (ChromExM). We applied ChromExM

to uncover how the pioneer factor Nanog interacts with chromatin and recruits Pol II to activate transcription during genome reprogramming after fertilization.

Nanog forms DNA-bound foci associated with Pol II recruitment and transcription

In zebrafish, Nanog is required for genome reprogramming and transcriptional activation after fertilization (8, 9, 12, 13). To investigate the molecular organization of transcriptional activation during genome activation, we analyzed the spatial organization of Nanog from the 32- to the 512-cell stage when transcription is activated. Live imaging of Nanog using a LlamaTag (14) revealed that Nanog formed clusters associated with the very early transcription of microRNA-430 (miR-430) (47% of miR-430 transcription sites contain Nanog foci) (Fig. 1, A and B; fig. S1, A to C) (15–18). Quantification of Nanog fluorescence revealed that these foci increased the local Nanog concentration 2.5- to 4-fold (fig. S1B), which is consistent with the occurrence of transcription factor and coactivator foci or hubs observed during embryogenesis and in cultured cells (19–28). We also observed that Nanog foci were associated with Pol II elongation, which is consistent with previous observations (16, 17, 22, 25, 27–30). Within a cell cycle, the formation of Nanog foci preceded Pol II elongation (Fig. 1, C and D), as visualized with a genetically encoded mintbody that detects elongating Pol II (Pol II pSer2) (25). After Pol II elongation begins, Nanog foci become less intense, which suggests that Nanog clusters may be evicted or dispersed after initiating transcription. In maternal-zygotic Nanog mutants (MZ$nanog^{-/-}$) (8), Pol II foci are lost and overall levels are reduced at the 256-cell stage, which

confirms Nanog's role in Pol II recruitment transcriptional activation (fig. S1, D and E) (29). Mutating the Nanog homeodomain to prevent DNA binding abolished Nanog foci, which indicates that they form in a DNA-binding–dependent manner rather than strictly through protein–protein interactions (fig. S1, F to I). Thus, Nanog forms DNA-bound hubs that increase its local concentration and are associated with Pol II recruitment and transcriptional activation during genome reprogramming.

ChromExM achieves single-nucleosome resolution while preserving chromatin organization across scales

Next, we aimed to determine the underlying nanostructure and molecular organization of Nanog and RNA Pol II during chromatin reprogramming and transcriptional activation. To this end, we adapted the concept of pan-ExM (11) to include metabolic labeling of DNA and nascent RNA, along with antibody labeling to visualize the chromatin with nanometer resolution, hereafter termed ChromExM (Fig. 1, E and F). ChromExM involves the direct anchoring of biomolecules to a swellable hydrogel through the addition of acryloyl groups, which allows protein and nucleic acid retention during expansion (11). We achieved an average ~15× linear expansion factor of the nuclei in embryos (Fig. 1G), which corresponded to a ~4000-fold increase in nuclear volume and provided ~15-nm lateral resolution on a confocal microscope and ~3 nm in stimulated emission depletion (STED) super-resolution microscopy (Fig. 2).

Previous studies have reported conflicting results regarding the isotropy of ~4× to 8× expansion of chromatin (31, 32). To address whether chromatin structure is perturbed by physical expansion, we developed an assay in which a pattern of parallel stripes is photocleaved into biotin-labeled DNA before expansion and visualized after expansion (Fig. 2A; fig. S2, A and B; and materials and methods). If chromatin expands isotropically, then the relative position of chromatin chains should be preserved, and the photocleaved stripes will remain parallel after expansion. We observed that stripes generated before expansion remain parallel after expansion and show no significant variation in their spacing when compared with simulated perfectly straight stripes generated as controls (Fig. 2, B and C; fig. S2, C and D; and materials and methods). This indicates that chromatin expands isotropically and the relative spatial organization of chromatin is preserved across the nucleus at submicron to global length scales by ChromExM (Fig. 2, B and C).

The preservation of chromatin structure at the nucleosomal level depends, in part, on the mesh size of the hydrogel, which affects the positional uncertainty and anchoring frequency

[1]Department of Genetics, Yale University School of Medicine, New Haven, CT 06510, USA. [2]Department of Cell Biology, Yale University School of Medicine, New Haven, CT 06510, USA. [3]Department of Biomedical Engineering, Yale University, New Haven, CT 06510, USA. [4]Institute for Regenerative Medicine, Perelman School of Medicine, University of Pennsylvania, Philadelphia, PA 19104, USA. [5]Kavli Institute for Neuroscience, Yale University School of Medicine, New Haven, CT 06510, USA. [6]Department of Physics, Yale University, New Haven, CT 06510, USA. [7]Nanobiology Institute, Yale University, West Haven, CT 06477, USA. [8]Yale Stem Cell Center, Yale University School of Medicine, New Haven, CT 06510, USA. [9]Yale Cancer Center, Yale University School of Medicine, New Haven, CT 06510, USA.

*Corresponding author. Email: mark.pownall@yale.edu (M.E.P.); liyun.miao@yale.edu (L.M.); antonio.giraldez@yale.edu (A.J.G.)
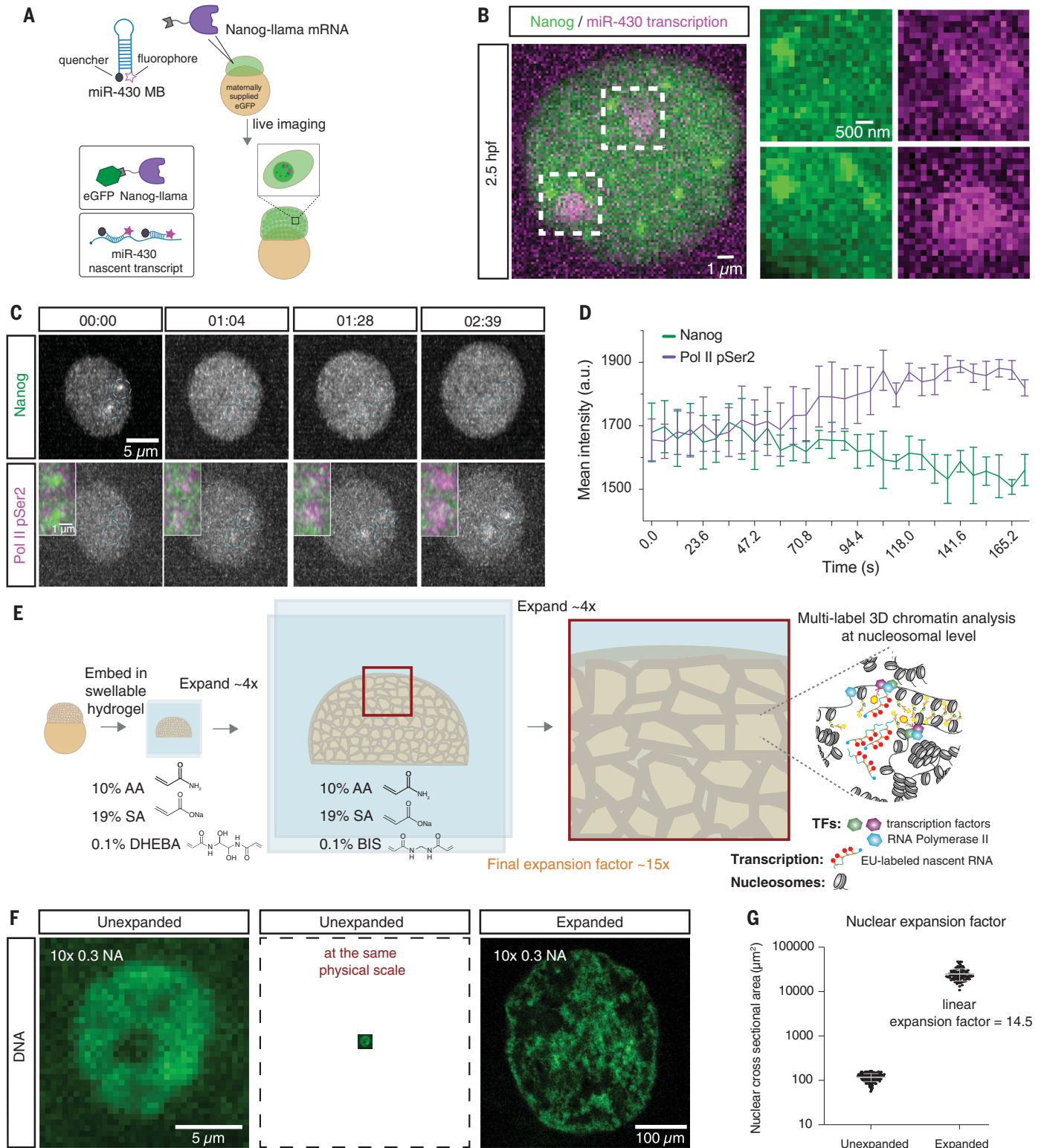
Fig. 1. Nanog forms DNA-bound foci associated with zygotic transcription.
(**A**) Schematic that details how Nanog and miR-430 transcription were visualized in living embryos. eGFP, enhanced green fluorescent protein. (**B**) Live imaging shows Nanog foci associated with miR-430 transcription at 2.5 hpf. $n = 10$ nuclei. (**C**) Live imaging shows Nanog foci are formed and disappear before Pol II elongation at = 2.75 hpf. $n = 2$ nuclei, 1 embryo. (**D**) Quantification of fluorescence intensity in (C). a.u., arbitrary unit. (**E**) Schematic that shows the process of ChromExM and expected results. AA,

acrylamide; BIS, N,N′-methylenebis(acrylamide); DHEBA, N,N′-(1,2-dihydroxyethylene) bisacrylamide; EU, 5-ethynyl uridine; SA, sodium acrylate. (**F**) Unexpanded and expanded nuclei from two unrelated embryos stained for DNA and imaged with a 10× 0.3 numerical aperture (NA) objective demonstrate the enhanced resolution provided by ChromExM. Scale bar is not corrected for the expansion factor. (**G**) Quantification of the nuclear expansion factor determined by measuring the nuclear cross-sectional area. $n = 171$ unexpanded nuclei from 3 embryos and 104 expanded nuclei from 17 embryos.

Fig. 2. ChromExM preserves chromatin architecture and resolves chromatin fibers and individual nucleosomes.
(**A**) Schematic that shows how the chromatin is painted with photocleaved (PC) stripes to detect perturbations after expansion. (**B**) Expanded nucleus that shows that PC stripes remain parallel and sharp after expansion. The image is a maximum intensity projection of several z-slices. n = 20 nuclei from 3 embryos. (**C**) Quantification of relative interstripe distance in PC stripes versus a simulated control (methods) shows minimal variation in the spacing between stripes after expansion. n = 3 nuclei from 3 embryos. (**D**) Schematic of in vitro–assembled nucleosome arrays. (**E**) ChromExM image (left) that shows nucleosome arrays with H3 staining and EM image of nucleosome arrays with a similar conformation as the expanded array. Red scale bar is not corrected for the expansion factor. (**F**) ChromExM image with metabolic DNA labeling at 2.75 hpf that shows individual chromatin fibers and a schematic of chromatin. n = 6 nuclei, 5 embryos. (**G**) H3 staining imaged with confocal and STED microscopy resolves individual nucleosomes. n = 468 nucleosomes; 3 nuclei from 2 embryos.
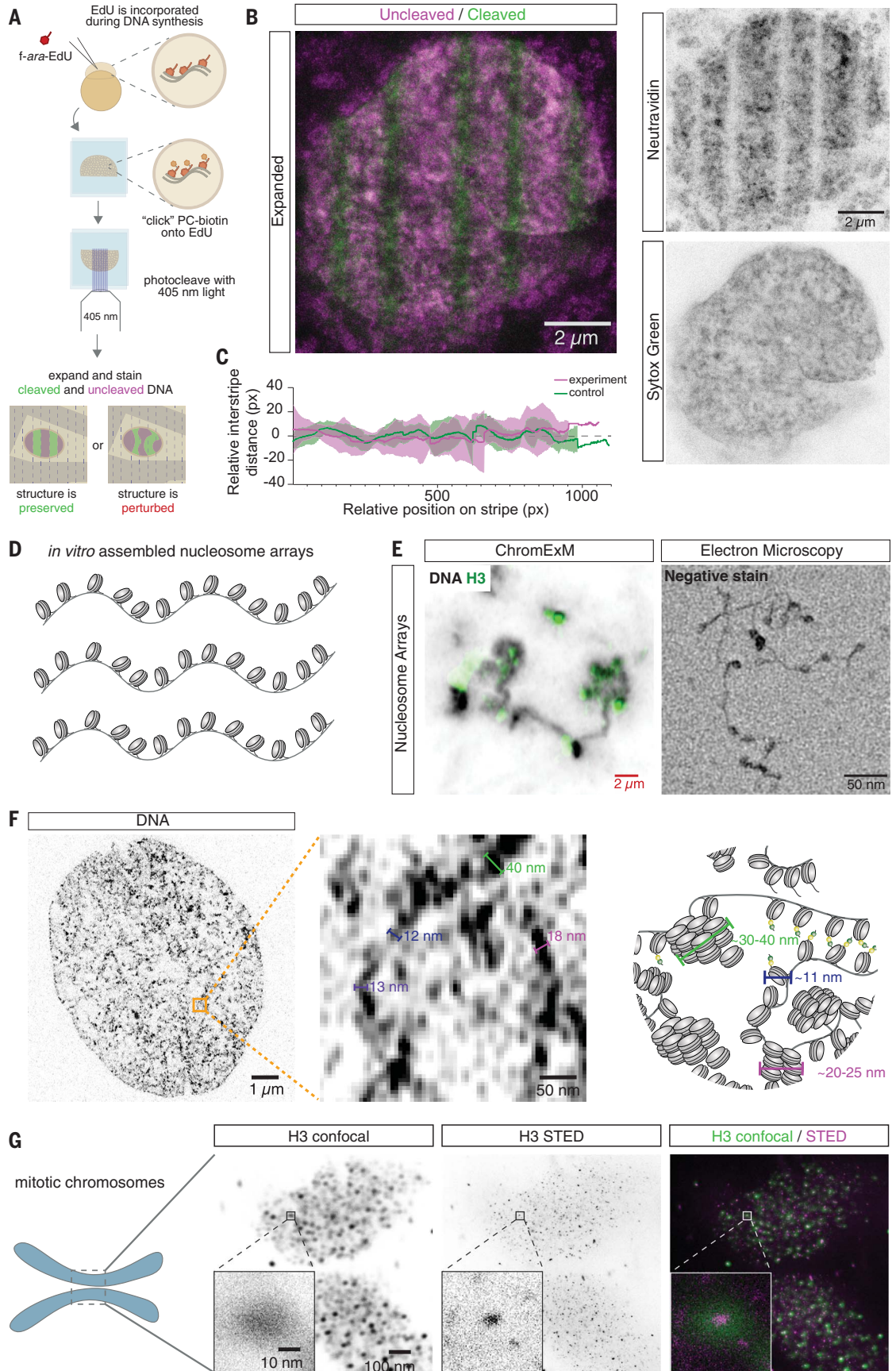
of biomolecules to the gel (33). To determine whether chromatin structure is maintained at the nucleosome scale, we measured the mesh size of our swellable hydrogel by assessing the mobility of differently sized molecules in the gel using fluorescence recovery after photobleaching (fig. S3, A to E) (34). We observed that a 3000 molecular weight (MW) dextran recovered quickly after photobleaching with a diffusion coefficient of 0.72 μm²/s, but histone H1 and a 2,000,000 MW dextran did not recover (fig. S3, A to E). These results demonstrate that the mesh size is small enough to prevent rapid diffusion of the ~32-kDa H1 protein, which suggests that the gel polymer can anchor the chromatin with subnucleosomal resolution. To functionally test this, we compared ChromExM and electron microscopy (EM) of in vitro–assembled nucleosome arrays containing 13 nucleosomes along 2.7 kb of DNA (Fig. 2, D and E; fig. S3, F and G) (35). We observed a similar organization of nucleosome arrays in ChromExM and unexpanded EM, with an average of 12.7 and 12.5 nucleosomes detected per array, respectively (Fig. 2E and fig. S3, F to H). Taken together, these results demonstrate that the local chromatin organization can be maintained at the nucleosomal scale during ChromExM.

To visualize chromatin, we metabolically labeled the DNA with (2′S)-2′-deoxy-2′-fluoro-5-ethynyluridine (f-ara-EdU) (36), followed by fluorescent picolyl azide detection after expansion (37). This approach was more photostable than the intercalating dye SYTOX Green and increased the labeling intensity ~45-fold compared with standard azides (fig. S3, J to L), which improved chromatin labeling to overcome the effects of molecular decrowding and reduced brightness caused by the ~4,000-fold volumetric expansion. This approach resolved chromatin fibers in the nucleus (Fig. 2F) with similar diameters (<12 to 40 nm) to those determined by EM (10). Nucleosomes are ~10 nm in size, which is at the resolution limit of confocal microscopy after ChromExM. Therefore, we performed STED microscopy with ChromExM to improve the resolution by an additional factor of approximately five, which approached <3-nm lateral resolution, and demonstrated that ChromExM can resolve individual nucleosomes by using histone H3 immunostaining and confocal microscopy (~80% of nucleosomes detected by confocal are individual nucleosomes by STED) (Fig. 2G and fig. S3I). The combination of ChromExM with STED provides fast multimodal molecular imaging of the chromatin that approaches <3-nm resolution.

Visualizing interactions between nucleosomes and the pioneer factor Nanog

We used ChromExM to determine the underlying nanoscale organization of transcription hubs during genome activation by visualizing the molecular-scale interactions among the pioneer factor Nanog (8, 9), nucleosomes, and Pol II at 4 hours post fertilization (hpf). To analyze how Nanog interacts with chromatin, we costained for Nanog and H3 and visualized an average of 88,619 and 104,347 individual particles of Nanog and H3 per nucleus, respectively, with a false-detection rate of 0.05% for identifying Nanog particles (Fig. 3, A to D; fig. S4, A to G; and movie S1). Quantitative analysis of the spatial organization of Nanog and H3 particles revealed several classes of Nanog–nucleosome conformations (Fig. 3, B to G; fig. S4, A to E and H to I; and materials and methods). In the first class, Nanog was closely associated with nucleosomes (<20 nm distance between Nanog and H3), with 2.0% of H3 and 3.3% of Nanog particles falling into this group (Fig. 3, B and E, and fig. S4A), which likely indicates a bound state in which Nanog is potentially initiating chromatin opening. In the second class, a subset of class 1, Nanog clusters were bound to a nucleosome (>1 Nanog particle within 20 nm and additional Nanog particles within 50 nm), which represents recruitment of multiple Nanog particles to the same chromatin region (0.06% of H3, 0.2% of Nanog) (Fig. 3, C and F, and fig. S4, B and B′). The third class contained Nanog particles distantly associated with nucleosomes (20 to 100 nm away from each other) (26.9% of H3, 39.7% of Nanog), which potentially indicates chromatin regions already opened by Nanog (Fig. 3, D and G, and fig. S4C). The fourth class contained nucleosomes and Nanog not closely associated with each other (>100 nm away) (71.2% of H3, 57.0% of Nanog) (fig. S4, D and E). Our analysis identified 88,619 Nanog particles per nucleus, which is consistent with the number of chromatin immunoprecipitation followed by sequencing (ChIP-seq) peaks (~40,000) identified at a similar stage in zebrafish (8, 38). These measurements are likely the lower bounds of Nanog–nucleosome interactions considering that some nucleosomes may not be detected here. Taken together, we are able to characterize pioneer factor–nucleosome organization during chromatin opening.

RNA Pol II forms string nanostructures associated with nascent RNA

To understand how transcription is organized during chromatin reprogramming, we used ChromExM to visualize Nanog and Pol II phosphoserine 5 (pSer5), which is deposited on Pol II after recruitment to the promoter (Fig. 3, H to K; fig. S5, A to C; and movie S2) (39–41). We detected an average of 27,503 Pol II particles per nucleus, which have characteristics consistent with single-molecule detection on the basis of their size and homogeneous intensity (fig. S5, D to G). Globally, the average distance between Pol II pSer5 and Nanog particles was 94 nm (Fig. 3L), with 19% of Pol II pSer5 particles being within 50 nm of Nanog particles, consistent with Nanog's role in Pol II recruitment (8). However, we observed that Pol II exhibited three distinct types of organization (Fig. 3, I to K, and fig. S5, A, B, C, and H). The first class involved large groupings of interspersed Pol II pSer5 and Nanog particles (412 Pol II pSer5 particles and 100 Nanog particles on average, 132-μm mean length) arranged like beads on a string, which we refer to as class 1 strings and occurred twice per nucleus in 86% of nuclei observed (Fig. 3, I and M to O; fig. S5A). RNA fluorescence in situ hybridization (RNA FISH) for miR-430 revealed that class 1 strings represent sites of active miR-430 transcription (Fig. 3, P and Q; fig. S6, A to C). To validate this result, we assembled the highly repetitive miR-430 locus using single haploid embryo long-read genome sequencing and identified a single, continuous ~550-kb miR-430 locus (fig. S7, A to F), which corresponded to an estimated length of ~200 μm, which is consistent with the 132-μm length of class 1 strings (Fig. 3O). This locus has been estimated to have >300 promoters capable of transcribing primary miR-430 transcripts (42), which is consistent with the ~1800 mature miR-430 genes detected in our assembly (fig. S7, C and D). Similarly, we detect ~400 Pol II pSer5 particles in class 1 strings, which likely represent binding at these promoters (Fig. 3M). The string-like structure that connects Pol II and Nanog particles is consistent with Pol II and Nanog binding profiles observed by ChIP-seq at this locus (fig. S7, G and H) (8, 12). Additionally, miR-430 RNA FISH signal and class 1 strings are lost in miR-430⁻/⁻ embryos (figs. S6, A and B, and S8, A and B) (43), which we confirmed lack all miR-430 genes using long-read genome sequencing (fig. S7, C to F). Together, these results demonstrate that class 1 strings show the nanoscale organization of the transcriptionally active miR-430 cluster (16, 17).

The second class of Pol II pSer5 organization involved multiple Pol II particles organized into strings with an average length of 831 nm (2 to 70 particles; mean of 4 particles per string) (Fig. 3, J and M to O; fig. S5, B and H). In this class, 37% of Pol II pSer5 particles were within 50 nm of Nanog particles, consistent with Nanog's role in Pol II recruitment. We hypothesized that these linear class 2 Pol II pSer5 strings represent individual genes loaded with Pol II arranged in single-file lines. Class 2 strings are still present in miR-430⁻/⁻ embryos (fig. S8, B and C), which indicates that they represent other transcribed genes (8). This processive organization of Pol II is reminiscent of active transcriptional elongation. In other cases, we observed branched Pol II pSer5 strings (Fig. 3J and fig. S5, B and H), which is consistent with the
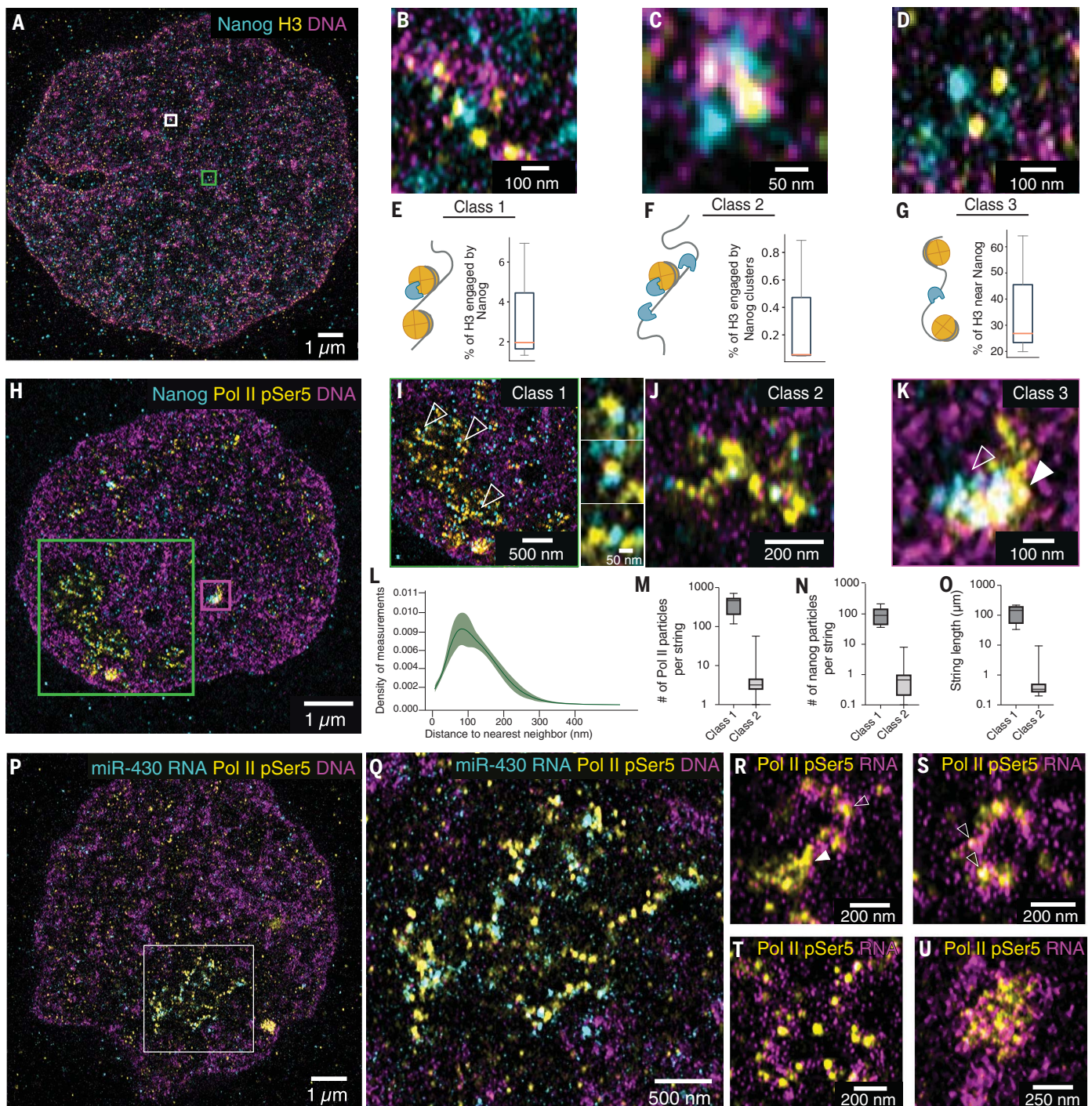
Fig. 3. Visualizing the nanoscale organization of Nanog, nucleosomes, Pol II, and transcription. (**A** to **D**) Representative images showing Nanog and H3 staining at 4 hpf; (B) represents class 1 organization. (C) represents the white boxed region in (A) and shows class 2 organization. (D) represents the green boxed region in (A) and shows class 3 organization. $n = 3$ nuclei from 2 embryos. (**E** to **G**) Box plots quantifying the percentage of H3 particles in each class of Nanog–H3 interactions. The median is denoted by the orange line. $n = 104,347$ distances. (**H** to **K**) Representative images showing Nanog and Pol II pSer5 staining at 4 hpf, $n = 7$ nuclei from 2 embryos. (I) represents the green boxed region in (H) and shows class 1 organization; areas indicated with arrowheads are magnified to the right. (J) represents class 2 organization. (K) represents the magenta boxed region in (H) and shows class 3 organization; arrowheads indicate regions enriched for Nanog (open arrowhead) and Pol II pSer5 (closed arrowhead). (**L**) Density plot of the distance to nearest neighbor for Nanog and Pol II pSer5 particles; $n = 169,866$ distances. (**M**) Box plots quantifying the number of Pol II pSer5 particles in class 1 ($n = 36$) and class 2 ($n = 5682$) strings. (**N**) Box plots quantifying the number of Nanog particles in class 1 and class 2 Pol II pSer5 strings. (**O**) Box plots quantifying the length of Pol II pSer5 strings in class 1 and class 2. (**P** and **Q**) ChromExM images showing Pol II pSer5 and miR-430 RNA detected by hybridization chain reaction RNA FISH at 4 hpf. (Q) represents the boxed region in (P). (**R** to **U**) Representative images showing nascent RNA and Pol II pSer5 at 4 hpf. $n = 7$ nuclei from 3 embryos. The closed arrowhead in (R) indicates a central Pol II pSer5 hub with an emanating string of individual Pol II pSer5 particles associated with nascent transcripts (open arrowhead). Open arrowheads in (S) indicate individual Pol II pSer5 particles.

transcription factory model in which multiple genes are in close proximity and share a regulatory Pol II hub (*29, 44, 45*). Indeed, we detected an average of 822 Pol II pSer5 strings per nucleus, which is consistent with the ~1700 active zygotic genes at 4 hpf we previously identified (*17*).

The third class of Pol II organization involved "macroclusters" (Fig. 3K and fig. S5C) similar to those previously observed by super-resolution imaging (*20–22*). We detected an average of 28 Pol II pSer5 macroclusters per nucleus. In cases in which these macroclusters were occupied by both Nanog and Pol II, we were able to resolve distinct regions within the cluster occupied solely by Nanog and Pol II (Fig. 3K and fig. S5C), as if the two factors were tethered on distinct DNA elements. These examples are consistent with Nanog bound to enhancers that reside in close proximity (<50 nm) to Pol II bound at the promoter (*8, 38*). Similarly, we observe all three classes of Pol II pSer5 organization during the minor wave of genome activation at 2.5 hpf, although there were fewer active sites, which is consistent with lower levels of transcription at this time (fig. S9, A to H) (*16, 17, 46*). This suggests that each class of Pol II organization represents a generalizable state of Pol II organization broadly used throughout genome activation. At 4 hpf, we observed that there are an average of 5.3 Pol II particles within 200 nm of each Nanog particle among all three classes, which suggests that multiple Pol IIs are recruited by Nanog. Among the macroclusters, we also observed multiple cases in which a string of RNA Pol II emanated from the cluster (Fig. 3K), which raises the question of how these two distinct Pol II pSer5 structures may function.

We hypothesized that Pol II pSer5 strings represent actively transcribing Pol II, which has exited the shared regulatory hub where Nanog, Pol II, and potentially other coactivators congregate to control gene expression. To test this, we combined metabolic RNA labeling using 5-ethynyl uridine with ChromExM labeling for Pol II pSer5 and observed nascent transcripts associated with all three classes of Pol II pSer5 structures (Fig. 3, R to U; fig. S10, A to F; and movie S3). We observed a wide range of transcription levels associated with the Pol II pSer5 strings, which suggests that they may encompass actively transcribed gene bodies as well as paused promoters (fig. S10G). The organization of these transcriptionally active Pol II pSer5 strings is consistent with Pol II elongation along the gene body of individual genes, for which we visualized multiple Pol II pSer5 particles that extrude nascent transcripts in concert (Fig. 3, R to T; fig. S10, A, B, C, E, and F). Taken together, these results support a model in which Nanog and Pol II clusters are in close physical proximity

and form a regulatory hub that activates transcription as Pol II exits the hub to form a string along the gene body (Fig. 3R and fig. S10A).

Enhancers and promoters are kicked apart by transcription elongation

Next, we assessed whether these Pol II pSer5 structures are formed in a transcription-dependent manner (Fig. 4, A to H; fig. S11, A to G; and movie S4). Inhibiting transcription elongation with α-amanitin (*47–50*) led to a strong reduction of Pol II pSer5 string length (66% reduction; $P = 0.002$) (Fig. 4, C, D, G, H, and I) and a mild reduction in the size and number of Pol II macroclusters (26.3% reduction in number; $P = 0.0304$) (Fig. 4J and fig. S11H) without reducing Pol II particle count (fig. S11I). Taken together, these data indicate that Pol II pSer5 strings represent transcription elongation, whereas Pol II pSer5 macroclusters may function as a regulatory hub formed independently of elongation.

We also observed that Nanog and Pol II particles were closer after treatment with α-amanitin (Fig. 4K; median distance 106 nm versus 66 nm; $P < 0.001$), with more Pol II pSer5 particles surrounding each Nanog particle (Fig. 4L; 3.1 versus 7.6 Pol II per Nanog; $P < 0.001$). Similar behavior between Nanog and Pol II was observed when transcription was inhibited in $miR\text{-}430^{-/-}$ embryos (fig. S11J), which suggests that these changes occur at multiple loci in the genome. We explain these results with the following model: Nanog first recruits Pol II to enhancer–promoter hubs, which brings them into close proximity; then Pol II exits the regulatory hub in the form of Pol II pSer5 strings, which transcribes the gene body (Fig. 4). When transcription elongation was inhibited, we observed an increase in the stoichiometry and proximity of Nanog-Pol II particles, which is consistent with Pol II stalling at the promoter and the stabilization of enhancer and promoter interactions.

To test this model, we performed ChIP-seq for Pol II pSer5 in wild-type and α-amanitin–treated embryos and observed extensive pileup of Pol II at promoters when blocking transcription (Fig. 4M and fig. S11K). As predicted from our ChromExM results, Pol II pSer5 accumulated at Nanog-bound enhancers and other accessible sites (Fig. 4, N and O; fig. S11, L and M), yet these regions are not enriched for RNA Pol II in wild-type embryos (Fig. 4, N and O; fig. S11, L and M) (*8*). These results can be explained by a model in which enhancer–promoter contacts are transient, consistent with the kiss-and-run model (*21*), and there is, therefore, a larger mean distance between Nanog and Pol II (Fig. 4K). However, in the absence of transcriptional elongation, Pol II is continuously brought to the promoter and remains in close proximity to the enhancer as observed by ChIP-seq. This is further supported

by the increase in the number of Pol II particles that surround each Nanog particle (Fig. 4L). On the basis of these data, we propose a modified version of the kiss-and-run model termed "kiss and kick," in which transcription itself kicks away the enhancer from the promoter as Pol II elongates (Fig. 4P). This would explain why we observe a stabilization of Poll II in close proximity to Nanog-bound enhancers when elongation is inhibited.

Discussion

Here, we developed ChromExM for multimodal super-resolution chromatin imaging by physically enlarging biological samples to achieve nucleosomal resolution. We demonstrate that chromatin organization is preserved and developed an improved metabolic labeling strategy for chromatin imaging (Fig. 2). ChromExM provides markedly higher resolution than previous ExM applications for chromatin imaging (~3 to 15 nm versus ~65 nm) (*31*). Other methods to visualize chromatin, such as ChromEMT (*10*), lack multimodal labeling, and the resolution of single-molecule localization microscopy is limited by the size of the fluorescent labels (~20 nm for primary and secondary antibody), which becomes negligible in ChromExM given that labels are applied after expansion (*11*). Although ChromExM provides substantial technical advances, it requires bright and photostable fluorescent labeling and chemical fixation, which may affect the appearance of certain structures. Future methods will be needed to identify specific loci through DNA FISH compatible with ChromExM to investigate specific regulatory structures at individual genes.

We used ChromExM to characterize the nanoscale organization of the pioneer factor Nanog and RNA Pol II as they activate transcription during genome activation. Although previous studies have shown how pioneer factors direct chromatin opening in vitro (*51, 52*) and organize into hubs in vivo (*19, 28, 53, 54*), the nanoscale organization of such hubs has remained unclear. ChromExM revealed that Pol II shows three types of organization during genome activation and is intimately associated with Nanog (Fig. 3, H to K). Previous studies have shown that transcription factors (TFs) such as Oct4, Brd4, and Mediator form clusters associated with superenhancers (*21, 23, 24*). With the resolution of ChromExM, we can now resolve how Nanog and Pol II often occupy distinct regions within transcription hubs, which is consistent with their binding at enhancers and promoters that are in close contact.

How enhancers and promoters are organized to activate transcription is central to understanding gene regulation. Previous reports have concluded that enhancer–promoter contact is correlated (*55*), anticorrelated (*56*), or unrelated (*57*) with transcription, which
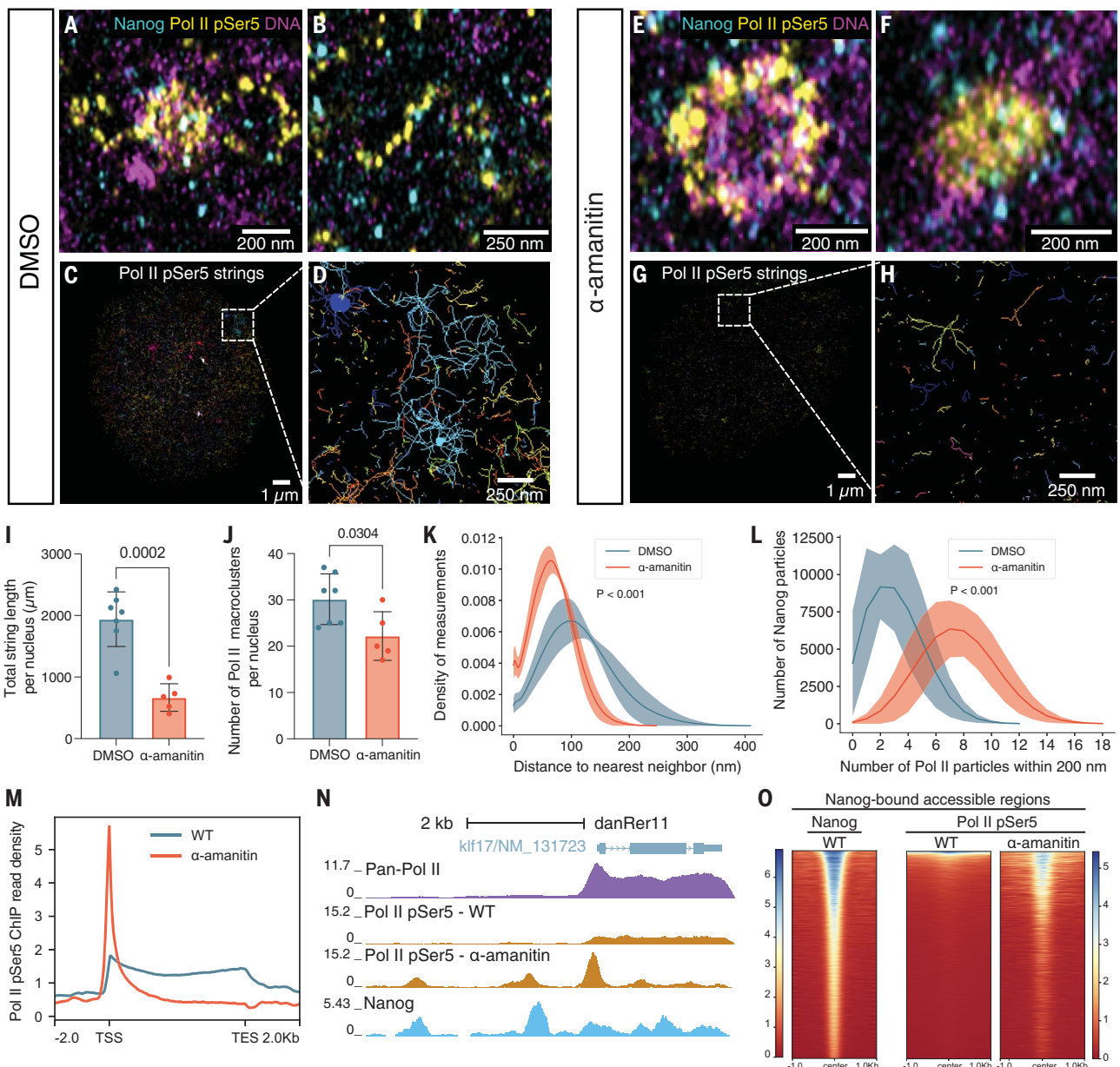
Fig. 4. Nanog-bound enhancers and Pol II-bound promoters are kicked apart by transcription elongation. (**A** and **B**) Representative images of Nanog and Pol II pSer5 in dimethyl sulfoxide (DMSO)–treated embryos at 4 hpf. *n* = 6 nuclei from 2 embryos. (**C** and **D**) Visualization of Pol II pSer5 strings identified in DMSO-treated embryos at 4 hpf. (**E** and **F**) Representative images of Nanog and Pol II pSer5 in α-amanitin–treated embryos. (**G** and **H**) Visualization of Pol II pSer5 strings identified in α-amanitin–treated embryos. (**I**) Quantification of total Pol II pSer5 string length per nucleus in DMSO- and α-amanitin–treated embryos. *P* = 0.0002; unpaired *t* test. (**J**) Quantification of the number of Pol II pSer5 macroclusters detected in DMSO- and α-amanitin–treated embryos. *P* = 0.0304; unpaired *t* test. (**K**) Density plot of the distance to nearest neighbor for Nanog to Pol II pSer5 particles in DMSO- and α-amanitin–treated embryos. *n* = 221,335 and 229,706 distances, respectively. *P* < 0.001; Mann-Whitney *U* test. (**L**) Histogram showing the number of Pol II pSer5 particles within 200 nm of each Nanog particle in DMSO- and α-amanitin–treated embryos. *P* < 0.001; Mann-Whitney *U* test. (**M**) Line plot showing Pol II pSer5 binding across gene bodies ±2 kb at zygotic genes in wild-type (WT) and α-amanitin–treated embryos. TES, transcription end site TSS, transcription start site. (**N**) Representative genome tracks of pan-Pol II, Pol II pSer5, and Nanog binding showing accumulation of Pol II pSer5 at the promoter and Nanog-bound enhancers in the presence of α-amanitin. (**O**) Heatmaps showing Pol II pSer5 binding at Nanog-bound accessible regions in WT and α-amanitin–treated embryos. Regions are ranked by Nanog ChIP-seq signal. (**P**) Schematic showing the kiss-and-kick model.

leaves the question of how enhancer–promoter contact is related to transcription unanswered. Three models have been proposed to explain how enhancers and promoters interact to control gene expression: (i) stable contact between enhancers and promoters, (ii) a dynamic kissing model with transient enhancer–promoter contacts, and (iii) a TF activity gradient in which TFs diffuse from enhancers to promoters rather than requiring physical contact (*58*). Our results are not consistent with models (i) and (iii) and lead to a model in which Nanog can form clusters at enhancers, coming into physical proximity with Pol II at the promoter and eventually triggering transcription, which we observed outside of this shared regulatory hub as strings of Pol II. Consistent with this model, we found that Pol II strings were substantially reduced when elongation was inhibited, which coincided with an accumulation of Pol II at promoters and in Nanog-bound enhancers and indicates that the enhancer and promoter were stabilized in close contact (Fig. 4, A to P). Taken together, these results suggest that Pol II elongation displaces enhancer–promoter contacts and lead us to propose the kiss-and-kick model. In this model, the dynamic association between the enhancer and promoter is kicked apart during elongation. This effect can be caused by either transcription elongation or the nascent RNAs that have been shown to dissolve Mediator condensates (*59*). The kiss-and-kick model could also explain transcriptional bursting (*60*), as elongation would be triggered in intervals while the enhancer and promoter are in contact and then paused after elongation kicks away the enhancer.

REFERENCES AND NOTES

1. N. L. Vastenhouw, W. X. Cao, H. D. Lipshitz, *Development* **146**, dev161471 (2019).
2. M. T. Lee, A. R. Bonneau, A. J. Giraldez, *Annu. Rev. Cell Dev. Biol.* **30**, 581–613 (2014).
3. V. Yartseva, A. J. Giraldez, *Curr Top Dev Biol.* **113**, 191–232 (2015).
4. K. N. Schulz, M. M. Harrison, *Nat. Rev. Genet.* **20**, 221–234 (2019).
5. C. L. Wike et al., *Genome Res.* **31**, 981–994 (2021).
6. A. Soufi, G. Donahue, K. S. Zaret, *Cell* **151**, 994–1004 (2012).
7. A. Soufi et al., *Cell* **161**, 555–568 (2015).
8. L. Miao et al., *Mol. Cell* **82**, 986–1002.e9 (2022).
9. M. Pálfy, G. Schulze, E. Valen, N. L. Vastenhouw, *PLOS Genet.* **16**, e1008546 (2020).
10. H. D. Ou et al., *Science* **357**, eaag0025 (2017).
11. O. M'Saad, J. Bewersdorf, *Nat. Commun.* **11**, 3850 (2020).
12. M. T. Lee et al., *Nature* **503**, 360–364 (2013).
13. M. Leichsenring, J. Maes, R. Mössner, W. Driever, D. Onichtchouk, *Science* **341**, 1005–1009 (2013).
14. J. P. Bothma, M. R. Norstad, S. Alamos, H. G. Garcia, *Cell* **173**, 1810–1822.e16 (2018).
15. P. Heyn et al., *Cell Rep.* **6**, 285–292 (2014).
16. Y. Hadzhiev et al., *Nat. Commun.* **10**, 691 (2019).
17. S. H. Chan et al., *Dev. Cell* **49**, 867–881.e8 (2019).
18. A. J. Giraldez et al., *Science* **312**, 75–79 (2006).
19. M. Mir et al., *eLife* **7**, e40497 (2018).
20. W.-K. Cho et al., *eLife* **5**, e13617 (2016).
21. W.-K. Cho et al., *Science* **361**, 412–415 (2018).
22. I. I. Cisse et al., *Science* **341**, 664–667 (2013).
23. B. R. Sabari et al., *Science* **361**, eaar3958 (2018).
24. A. Boija et al., *Cell* **175**, 1842–1855.e16 (2018).
25. S. Uchino et al., *J. Cell Biol.* **221**, e202104134 (2022).
26. Y. Sato et al., *Development* **146**, dev179127 (2019).
27. S.-K. Huang, P. H. Whitney, S. Dutta, S. Y. Shvartsman, C. A. Rushlow, *Curr. Biol.* **31**, 5102–5110.e5 (2021).
28. K. Kuznetsova et al., *Curr. Biol.* **33**, 164–173.e5 (2023).
29. F. J. Iborra, A. Pombo, D. A. Jackson, P. R. Cook, *J. Cell Sci.* **109**, 1427–1436 (1996).
30. A. Pombo et al., *EMBO J.* **18**, 2241–2253 (1999).
31. E. L. Faulkner et al., *J. Cell Sci.* **135**, jcs259009 (2022).
32. S. P. Pernal et al., *Histochem. Cell Biol.* **153**, 469–480 (2020).
33. F. Chen, P. W. Tillberg, E. S. Boyden, *Science* **347**, 543–548 (2015).
34. J. Karvinen, T. O. Ihalainen, M. T. Calejo, I. Jönkkäri, M. Kellomäki, *Mater. Sci. Eng. C* **94**, 1056–1066 (2019).
35. M. A. Frederick et al., *Nat. Struct. Mol. Biol.* **30**, 31–37 (2023).
36. A. B. Neef, N. W. Luedtke, *Proc. Natl. Acad. Sci. U.S.A.* **108**, 20404–20409 (2011).
37. C. Uttamapinant et al., *Angew. Chem. Int. Ed.* **51**, 5852–5856 (2012).
38. C. Xu et al., *Dev. Cell* **22**, 625–638 (2012).
39. S. Buratowski, *Mol. Cell* **36**, 541–546 (2009).
40. H. Lu, L. Zawel, L. Fisher, J.-M. Egly, D. Reinberg, *Nature* **358**, 641–645 (1992).
41. S. Trigon et al., *J. Biol. Chem.* **273**, 6769–6775 (1998).
42. Y. Hadzhiev et al., *Dev. Cell* **58**, 155–170.e8 (2023).
43. Y. Liu et al., *PLOS ONE* **8**, e76387 (2013).
44. J. A. Mitchell, P. Fraser, *Genes Dev.* **22**, 20–25 (2008).
45. C. S. Osborne et al., *Nat. Genet.* **36**, 1065–1071 (2004).
46. M. Ugolini, K. Kuznetsova, H. Oda, H. Kimura, N. L. Vastenhouw, Targeted disruption of transcription bodies causes widespread activation of transcription. bioRxiv 517317 [Preprint]. 21 November 2022.
47. D. A. Bushnell, P. Cramer, R. D. Kornberg, *Proc. Natl. Acad. Sci. U.S.A.* **99**, 1218–1222 (2002).
48. A. L. Greenleaf, *J. Biol. Chem.* **258**, 13403–13406 (1983).
49. T. J. Lindell, F. Weinberg, P. W. Morris, R. G. Roeder, W. J. Rutter, *Science* **170**, 447–449 (1970).
50. D. A. Kane et al., *Development* **123**, 47–55 (1996).
51. M. Fernandez Garcia et al., *Mol. Cell* **75**, 921–932.e6 (2019).
52. E. Luzete-Monteiro, K. S. Zaret, *Curr. Opin. Struct. Biol.* **75**, 102425 (2022).
53. J. Dufourt et al., *Nat. Commun.* **9**, 5194 (2018).
54. M. M. Gaskill, T. J. Gibson, E. D. Larson, M. M. Harrison, *eLife* **10**, e66668 (2021).
55. H. Chen et al., *Nat. Genet.* **50**, 1296–1303 (2018).
56. N. S. Benabdallah et al., *Mol. Cell* **76**, 473–484.e7 (2019).
57. L. J. Mateo et al., *Nature* **568**, 49–54 (2019).
58. J. P. Karr, J. J. Ferrie, R. Tjian, X. Darzacq, *Genes Dev.* **36**, 7–16 (2022).
59. J. E. Henninger et al., *Cell* **184**, 207–225.e24 (2021).
60. A. Coulon, C. C. Chow, R. H. Singer, D. R. Larson, *Nat. Rev. Genet.* **14**, 572–584 (2013).
61. M. E. Pownall, C. E. Vejnar, A. J. Giraldez, Code for: Chromatin expansion microscopy reveals nanoscale organization of transcription and chromatin (1.0), Zenodo (2023); https://doi.org/10.5281/zenodo.7933370.

SUPPLEMENTARY MATERIALS

science.org/doi/10.1126/science.ade5308
Materials and Methods
Figs. S1 to S11
References (*62–101*)
Data S1 to S3
MDAR Reproducibility Checklist
Movies S1 to S4

View/request a protocol for this paper from *Bio-protocol*.

Chromatin expansion microscopy reveals nanoscale organization of transcription and chromatin

Mark E. Pownall, Liyun Miao, Charles E. Vejnar, Ons MSaad, Alice Sherrard, Megan A. Frederick, Maria D. J. Benitez, Curtis W. Boswell, Kenneth S. Zaret, Joerg Bewersdorf, and Antonio J. Giraldez

Editor's summary

The spatial organization of chromatin and specific factors within the nucleus regulates gene expression. To visualize nuclear organization at the molecular scale in developing embryos, Pownall *et al.* developed chromatin expansion microscopy (ChromExM), which drastically improves the resolution of light microscopy by physically expanding embryos embedded in a series of swellable hydrogels without distorting chromatin organization (see the Perspective by Stasevich and Kimura). This procedure enabled the visualization of individual nucleosomes and revealed how the pioneer factor Nanog interacts with them. The authors also observed RNA polymerase II nanostructures engaged in active transcription, and developed a "kiss and kick" model of enhancer-promoter interactions in which transcription elongation leads to the physical separation of enhancers and promoters. —DJ

View the article online
https://www.science.org/doi/10.1126/science.ade5308
Permissions
https://www.science.org/help/reprints-and-permissions

Use of this article is subject to the Terms of service